Entropy production in the Au + Au reaction between 150 and 800 A MeV

C. Kuhn, J. Konopka, J.P. Coffin, C. Cerruti, P. Fintz, G. Guillaume, A. Houari, F. Jundt, C. Maguire, F. Rami, et al.

Entropy production in the Au + Au reaction between $150A$ and $800A$ MeV

C. Kuhn,[12] J. Konopka,[5] J. P. Coffin,[12] C. Cerruti,[12] P. Fintz,[12] G. Guillaume,[12]
A. Houari,[12] F. Jundt,[12] C. F. Maguire,[12,*] F. Rami,[12] R. Tezkratt,[12,†] P. Wagner,[12] Z. Basrak,[14]
R. Čaplar,[14] N. Cindro,[14] S. Hölbling,[14] J. P. Alard,[3] N. Bastid,[3] L. Berger,[3] S. Boussange,[3]
I. M. Belayev,[9] T. Blaich,[8] A. Buta,[1] R. Donà,[7] P. Dupieux,[3] J. Erö,[2] Z. G. Fan,[4]
Z. Fodor,[2] R. Freifelder,[4‡] L. Fraysse,[3] S. Frolov,[9] A. Gobbi,[4] Y. Grigorian,[4] N. Herrmann,[6]
K. D. Hildenbrand,[4] S. C. Jeong,[4] M. Jorio,[3] J. Kecskemeti,[2] P. Koncz,[2] Y. Korchagin,[9] R. Kotte,[11]
M. Krämer,[4] I. Legrand,[1] A. Lebedev,[9] V. Manko,[10] T. Matulewicz,[12] G. Mgebrishvili,[10] J. Mösner,[11]
D. Moisa,[1] G. Montarou,[3] I. Montbel,[3] W. Neubert,[11] D. Pelte,[6] M. Petrovici,[1] S. Ramillien,[3]
W. Reisdorf,[4] A. Sadchikov,[10] D. Schüll,[4] Z. Seres,[2] B. Sikora,[13] V. Simion,[1] S. Smolyankin,[10]
U. Sodan,[4] K. M. Teh,[4] M. Trzaska,[6] M. A. Vasiliev,[10] J. P. Wessels,[4] T. Wienold,[6] Z. Wilhelmi,[13]
D. Wohlfarth,[11] and A. V. Zhilin[9]

[1]*Institute for Physics and Nuclear Engineering, Bucharest, Romania*
[2]*Central Research Institute for Physics, Budapest, Hungary*
[3]*Laboratoire de Physique Corpusculaire, Clermont-Ferrand, France*
[4]*Gesellschaft für Schwerionenforschung, Darmstadt, Germany*
[5]*Institut für Theoretische Physik der Universität Frankfurt, Frankfurt am Main, Germany*
[6]*Physikalisches Institut der Universität Heidelberg, Heidelberg, Germany*
[7]*Istituto Nazionale di Fisica Nucleare, Legnaro, Italy*
[8]*Universität Mainz, Mainz, Germany*
[9]*Institute for Experimental and Theoretical Physics, Moscow, Russia*
[10]*Kurchatov Institute for Atomic Energy, Moscow, Russia*
[11]*Forschungzentrum, Rossendorf, Germany*
[12]*Centre de Recherches Nucléaires, IN2P3-CNRS, Université Louis Pasteur, Strasbourg, France*
[13]*Institute of Experimental Physics, Warsaw University, Warsaw, Poland*
[14]*Rudjer Boskovic Institute, Zagreb, Croatia*

The entropy per nucleon (S/A) has been extracted for the Au $[(150–800)A$ MeV$]$ + Au reaction by using the phase I setup of the 4π facility at GSI, Darmstadt. The entropy has been obtained from the comparison of various observables characterizing the dM/dZ fragment multiplicity distributions, extending up to $Z \sim 15$, with those calculated with the quantum statistical model. It is the first time that S/A values are determined by considering the full ensemble of charged products detected in the reaction. Consistent values of S/A are found from different methods. These entropy values are shown to be fairly independent of the volume of the "participant" region considered. They are somewhat lower than those extracted in earlier works but are in good agreement with hydrodynamic calculations and suggest a low viscosity for the hot and dense nuclear matter.

PACS number(s): 25.75.+r, 25.70.Pq

I. INTRODUCTION

Heavy-ion reactions at intermediate energies are currently under intense investigation [1] because they are expected to provide information on the general properties of nuclear matter at densities and temperatures much higher than those extensively studied at the ground state density $\rho_0 \cong 0.16$ nucleon/fm^3 and around zero temperature. The experimental results show strong dynamical

---

*On leave from Vanderbilt University, Nashville, TN 37235.
†Present address: Texas A&M University, College Station, TX 77843.
‡Present address: Department of Radiology, University of Pennsylvania, Philadelphia, PA 19104.

effects [1,2], like various forms of the flow of nuclear matter, which require the use of theoretical macroscopic (hydrodynamic [1–4]) and microscopic (Boltzmann-Uehling-Uhlenbeck [5], Vlasov-Uehling-Uhlenbeck [6], Boltzmann-Langevin [7], Landau-Vlasov [8], quantum molecular dynamical model [9], etc.) treatments. This complicates considerably the task of inferring from the experimental observations the properties of equilibrated nuclear matter under well-defined thermodynamic conditions. On the other hand, recent studies of very central heavy-ion collisions have revealed new features which suggest that possibly global equilibrium may be reached under favorable experimental conditions. This would justify the use of statistical models to extract simple but very useful thermodynamic quantities such as entropy. Indeed, the baryonic entropy per nucleon (S/A) is inherently connected with the momentum as well as with

the real-space configuration. Thus an independent measurement of S/A will lead to information on the overall phase-space occupancy in the central heavy-ion reactions. Such a determination was first proposed by Siemens and Kapusta [10] who suggested correlating S/A to the deuteron to proton yield ratio, claiming that the relative proportions of d and p are established during the early stage of the reaction. They applied this method to the study of the Ne+NaF and Ar+KCl systems at $100A$ and $200A$ MeV. They suggested that such analyses should be extended to heavier systems and that excitation functions should be measured.

As shown in a recent work [11], midrapidity intermediate mass fragments (IMF's, $3 \leq Z \leq 12$) are produced with a substantial cross section in highly central Au+Au reactions performed at $150A$ MeV. An extension of this work to a large energy range [$(100–800)A$ MeV] has established that these IMF's represent an important fraction of the total charge of the events corresponding to the most central collisions at all energies [12].

In this work, pursuing these studies, we will show that the IMF multiplicity distributions are characterized, over a large domain of bombarding energy, by an exponential falloff when the "participant" part (cf. the participant-spectator picture) is actually selected, and furthermore that this behavior is fairly independent of the volume of this part, providing it is not too small, i.e., for central and semicentral collisions. Encouraged by these observations, assuming that a statistical equilibrium is reached, we have proceeded to an analysis of the IMF distributions in terms of the entropy created in the reactions. The baryonic entropy per nucleon is particularly attractive because, although being built in the early stage of the reaction, it is conjectured to be essentially preserved during the evolution of the nuclear system [13–16].

To understand the fundamentals of entropy production in violent heavy-ion reactions and their relevance to the present class of studies of hot and dense nuclear matter, it is worth recalling briefly how the entropy is supposed to be created according to the vast ensemble of experimental results treated in the dynamics of the nuclear collision framework. It is generally conjectured that relativistic heavy-ion reactions (above about $100A$ MeV) proceed in the schematic following way: (1) An excited zone is formed from the region of contact between projectile and target. In this region the available energy is shared as compression energy and thermal energy, the latter resulting from nucleon-nucleon collisions whose frequency depends on the nucleon mean free path and consequently on the density. This brings the system to a stage of higher temperature (T) and density (ρ) which lasts only a very short time. (2) Indeed, photons, electron pairs, and mesons are promptly emitted, while the nucleonic system expands and disassembles into light particles (n, p, d, t, and ^{3,4}He) and fragments. However, at bombarding energies below about $700A$ MeV the mesonic component appears to be negligible [17]. During this phase, the potential compression energy is mostly converted into kinetic energy which communicates a collective motion to the bulk of particles and fragments, i.e, the flow of nuclear matter. Only a little compression energy is supposed to

be transformed into thermal energy due to weak viscosity. During this phase, T drops considerably. (3) The system expands further and reaches a state of dilute density compared with the saturation density ρ_0, where the nuclear interaction among the constituents ceases, the so-called breakup or freeze-out density. From this point on, only unstable fragments may still decay, yielding eventually the particle and fragment distribution which is actually measured experimentally.

Globally, it would seem that most of the degrees of freedom are created in the early stage of the collision and that the high temperature and density of the nuclear system, which decrease rapidly as the reaction proceeds, cannot be conveniently used to describe the system under a thermostatic aspect. When looking for an observable which does not change much after the highest T and ρ stage has been reached, one may consider the entropy (S) which describes the degrees of freedom of the system and which is reputed to remain essentially constant over the expansion of the system [13–16]. It can be defined as

$$S = -k \sum_i P_i \ln P_i , \tag{1}$$

where k is the Boltzmann constant and P_i characterizes the probability of finding the system in a microstate i. If the system is at equilibrium, then all the microstates are equiprobable and a statistical entropy may be defined as $S = k \ln\Omega(E)$, where $\Omega(E)$ describes the macrostate of energy E containing the large ensemble of microstates.

Turning to the methods to derive the entropy, on a theoretical footing there was first the method suggested by Siemens and Kapusta [10], already mentioned before, which relates the entropy per nucleon to the deuteron to proton yield ratio R_{dp}:

$$S/A = 3.95 - \ln R_{dp} . \tag{2}$$

This assumes that proton and deuteron yields reach rapidly an equilibrium through the reaction $d + N \rightleftharpoons n + p + N$, where N is a spectator nucleon or a cluster. Then light clusters (t, ^{3,4}He) were included by considering their deuteron and proton clustering. A deuteronlike to protonlike ratio $\tilde{R}_{dp}$ was determined [18] as

$$\tilde{R}_{dp} = \frac{N_d + \frac{3}{2}(N_t + N_{^3\text{He}}) + 3N_{^4\text{He}}}{N_p + N_d + N_t + 2(N_{^3\text{He}} + N_{^4\text{He}})} \tag{3}$$

to replace R_{dp} in Eq. (2); N_i represents the multiplicities of the various species i ($p,d,\dots$).

To be valid, however, this method requires the neutron and proton abundances to be much larger than that of all the other species together, a hypothesis which appeared soon to be incorrect [15,18]. Indeed, it was shown that heavier clusters should also be taken explicitly into account [17,19–21] for the two following main reasons: (1) At relatively low energy, experimental results show that IMF's are emitted in a substantial amount; hence, the assumption that protons and neutrons dominate the chemical equilibrium stage is not correct. When ignoring the fragments, one neglects their binding and excitation energies and the energy balance of the system is distorted.

Moreover, the quantum statistical corrections [22] and finite volumes of the produced fragments are not accounted for. (2) Many of the IMF's are unstable; thus, they undergo particle decay, hence distorting the $\tilde{R}_{dp}$ ratio. Indeed, protons and neutrons are abundantly produced via evaporation subsequent to chemical breakup.

Thus it appears that entropy should be extracted from a quantum statistical treatment of nuclear fragmentation. Several models of this type exist; they treat the decay process on the basis of microcanonical, canonical, and grand canonical ensembles [17,19,20,23–28] or on the binary sequential decay [29–32]. All these models require assumptions on the internal states of the particles, their decay properties, and their coordinate and momentum-space distributions at the time of freeze-out, as well as their mutual interactions at that time. Therefore entropy determination is model dependent. However, this dependence is perhaps more on the parameter choice than on the conceptual approaches of the various models. A detailed comparison [21] of the classical microcanonical model [24] and of the quantum statistical grand canonical model [19] has shown good agreement for the description of the final states of central Ca+Ca and Nb+Nb collisions at $400A$, $1050A$, and $400A$, $650A$ MeV, respectively, as well as for the entropy per nucleon determination. Among the various models, the quantum statistical model (QSM) of Hahn and Stöcker [17,19,20] makes explicit predictions about the entropy readily usable by the experimentalist and which offers alternate methods to extract S/A. Therefore it has been used as a first approach to extract the entropy values in the Au+Au reactions studied here. Other determinations from other theoretical approaches will follow.

Turning now to the experimental side, entropy values determined from QSM analysis have been reported in the literature [33–39]. They are from a variety of measurements (different nuclear systems, projectile energies, and methods of extracting S/A) which makes conclusive comparisons rather difficult. They tend to increase from about 1.5 to about 3.5 over the $(50-1000)A$ MeV energy range and yield values which are higher than those calculated [17] with equations of state (with linear and quadratic dependences on the incompressibility modulus K) which best reproduce the experimental pion multiplicities. One reason for finding a larger entropy than predicted by dynamical models was due to impact parameter averaging in inclusive measurements as shown by Gutbrod *et al.* [35] and Doss *et al.* [37]. On the other hand, they appear clearly lower than those corresponding to full conversion of the center-of-mass energy into thermal energy, thus evidencing the existence of a large compression energy which manifests itself in the presence of collective degrees of freedom of the nucleon matter formed. However, so far, no measurements have included the complete fragment distribution in the determination of the entropy. Summing up, it is important to examine whether taking the IMF's explicitly into account leads to the same S/A values as in earlier works where they were neglected. Furthermore, considering simultaneously all light particles and IMF's is a stringent test for theory and models which has never been undertaken before.

It is the aim of this article to extract S/A from the Au+Au reaction, performed between $150A$ and $800A$ MeV. Complete distributions of particles and IMF's ($1 \leq Z \leq 15$) have been taken into account to extract various observables characteristic of these distributions and to compare them with those calculated with the QSM, thus allowing for an S/A determination. This analysis is a part of a new generation of experiments consisting of analyzing the fragment production and IMF properties in relativistic heavy-ion reactions [40]. The Au+Au system has been chosen in order (1) to have the largest possible highly excited participant zone (if referring to the participant-spectator description), thus "simulating" the infinite nuclear matter considered by the models, and (2) to allow the best possible selection of the participant zone formed in violent collisions.

Light isotope yields determined with ΔE-E telescope counters [41] and neutron yields obtained with the LAND detector [42] have been measured simultaneously, in a joint experiment, with the charged particles and fragments presented here. These two sets of data should also lead to an entropy determination for the Au+Au reaction which will be presented in separate future articles.

In the following we recall first the method based on the use of the QSM to extract the entropy values (Sec. II); then, the experimental setup is briefly described in Sec. III. The experimental results are presented in Sec. IV where a discussion about the criteria of the centrality of the reactions precedes the presentation of the IMF distributions. The analysis of the data in terms of the baryonic entropy is presented in Sec. V. The discussion (Sec. VI) will present comparisons with earlier entropy extractions and with theoretical expectations. Finally, a summary will be given (Sec. VII).

II. ENTROPY DETERMINATION METHOD WITH THE QUANTUM STATISTICAL MODEL

Since entropy determination is model dependent, it is worth recalling the main characteristics of the QSM [17,19,20] used in the present work and to describe the way the calculations are conducted. This model supposes the sudden disassembly (breakup) of a nuclear system at given temperature and density. Here, due to compression, the thermal energy stored in the system is not that corresponding to the total available energy in the center of mass but only to that of a fraction of it. The model calculates a distribution of residue products which should not be that at the moment of freeze-out, since the IMF's may decay afterward, but that which is eventually measured experimentally.

It is assumed that the decaying system is chemically and thermally equilibrated at the moment of breakup; i.e., it is characterized by a variety of species i, each considered as an ideal Fermi or Bose gas, in equilibrium and at a uniform temperature. The calculations consist of determining the yields n_i of the different species, distinguished by their Bose or Fermi character. These yields depend on their individual chemical potential μ_i, the mass m_i, and the statistical weight of the species; they also depend on T and on the available volume V and

hence on the breakup density. The fragment chemical potentials are taken as the sum of those of their constituents (neutron n and proton p) together with their proper binding energy E_i:

$$\mu_i = Z_i \mu_p + N_i \mu_n + E_i \ , \tag{4}$$

where E_i for a cluster i having Z_i protons and N_i neutrons is

$$E_i = Z_i m_p c^2 + N_i m_n c^2 - m_i c^2 \ . \tag{5}$$

The available volume V is related to the density, when the particles are considered as punctual, as

$$\rho_{\text{punct}} = A/V \ ; \tag{6}$$

it is also related to the total volume as

$$V_T = V + V_{\text{excl}} \ , \tag{7}$$

where the excluded volume $V_{\text{excl}} = A/\rho_0$ is that occupied by the nucleons considered as hard spheres of fixed volume. Thus the total volume is connected to the density as

$$\rho = A/V_T = \frac{\rho_{\text{punct}}}{1 + \rho_{\text{punct}}\rho_0^{-1}} \ . \tag{8}$$

Then the entropy can be extracted for a given species from the simple formula

$$E_i^{\text{therm}} = TS_i - P_i V + \mu_i n_i \ , \tag{9}$$

relating the entropy to the thermal energy E_i^{therm} of an ideal quantum gas. For a mixture of gases, considered at a temperature T, and taking into account the equation of state of an ideal gas of fermions or bosons $P_i V = \frac{2}{3} E_i^{\text{therm}}$, one obtains

$$S_i = \sum_i S_i = \sum_i \frac{P_i V + E_i^{\text{therm}} - \mu_i n_i}{T}$$
$$= \sum_i (\tfrac{5}{3} E_i^{\text{therm}} - \mu_i n_i)/T \ . \tag{10}$$

Practically, the method does not consist of making any assumption on the initial temperature of the system, but consists, for given T and ρ, to search for the μ_p and μ_n, which give, by solving the two equations

$$Z = \sum_i n_i Z_i \ , \tag{11}$$

$$N = \sum_i n_i N_i \ , \tag{12}$$

the correct ratio N/Z of the system considered.

In the present case, the binding energies of 861 states of nuclei $A \leq 25$ together with about 200 stable isotopes up to $A = 208$ have been included in the calculation. The binding energies have been taken from Ref. [43]. In the regime of high nuclear excitations, as is the case here, the population of states of very heavy nuclei is negligible; i.e., the yields are down by at least three orders of magnitude compared to protons. In the most relevant region ($A < 20$), only experimentally known states are included.

Very highly excited primordial clusters, which themselves may undergo a sequential evaporation, are not considered. The inclusion of such high-lying states may change somewhat the value of entropy; however it is not clear whether they should be included in an equilibrium calculation, because their average lifetimes may be shorter than the time scale of the equilibration process, and for this reason they have been left out. The inclusion of a larger number of states of moderately excited nuclei, which will decay by emission of very light particles, is not expected to change the conclusion on the cluster observables since it will not lead to a large change of the IMF distributions.

Thus, concretely, on the one hand, one calculates with the QSM, for given T and ρ, the Z distributions determined by the n_i yields. These distributions exhibit approximately an exponential falloff and can be characterized by different observables such as the slope parameter and the average Z value. All these observables are related to the entropy, as will be shown in the next section. On the other hand, one can extract the same quantities from the experimental distributions, compare them to the calculated ones, and thus determine the entropy value.

It is essential to keep in mind that *no specific assumptions* are made about the initial thermal energy of the system before performing these statistical calculations. The method consists of finding the best possible agreement between the experimental Z distribution and the few theoretical distributions pertaining to the whole ensemble obtained in varying T and ρ. Thus, as long as no hypotheses are made neither on the density nor on the temperature, no unique value of S can be determined.

III. EXPERIMENTAL SETUP

The Au ion beam was delivered by the rapid-cycling synchrotron SIS, at GSI, Darmstadt. The experiments were performed at bombarding energies of $150A$, $250A$, $400A$, $600A$, and $800A$ MeV. The beam intensities were typically of 10^5 ions/s. Targets of 0.5% (for lower energies) up to 2% (for higher energies) interaction length (i.e., 200 mg/cm^2 for 0.5%) were used. An average of 10^6 events was collected at each energy.

The measurements were performed with the phase I setup of the 4π facility (FOPI). This apparatus has been described in detail elsewhere [40,44]. It consists of a highly segmented (764 elements) plastic scintillator wall yielding, through individual readouts, energy loss (ΔE), time of flight (τ), and polar (θ) and azimuthal angles of the detected ions. To achieve low detection energy thresholds, a shell of 188 thinner ΔE detectors is mounted in front of the scintillators, and the fragments travel from the target to the detector through a He bag. This ensemble spans the $1° \leq \theta \leq 30°$ domain and offers full azimuthal coverage. The combined ΔE-τ information allows the Z identification of the fragments, which, in the present experiments, could be extended up to $Z \sim 15$.

The acceptance and lower energy thresholds characterizing the apparatus have been discussed also in a previous article [44]. They depend on Z but also on θ because the

detector setup is different below and above 6°. These effects require some correction of the measured yields, essentially at incident energy less than $250A$ MeV. They are discussed further on in this presentation (cf. Sec. IV B).

IV. EXPERIMENTAL RESULTS

A. Centrality selection

The first task is to select, with the lowest possible bias, the particles and IMF's emitted from the participant zone formed in highly central collisions. Following earlier methods [45–47], we have selected the following events. (1) The charged particle multiplicity (PM), measured in the polar angle range $7° \leq \theta \leq 30°$ is the highest, i.e., the bin of multiplicity starting at half of the distribution-plateau value and onward, the so-called PM5 cut. Peripheral (PM1,PM2) and semicentral (PM3,PM4) events may be defined by dividing the lower multiplicity space into equal fractions. (2) The transverse momentum directivity [46,47]

$$D = \left[\left| \sum_i^{M_c} \mathbf{p}_t \right| \middle/ \sum_i^{M_c} \left| \mathbf{p}_t \right| \right]_{y_i \geq y_{c.m.}} \quad (13)$$

is taken as ≤ 0.2; i.e., the transverse momentum of the various fragments within an event are azimuthally balanced in the forward hemisphere. This generates the so-called PM5D1 cut, already used in a previous work [11] to select events from highly central collisions. Another relevant criterion [48] in the present case, may be the so-called E_{rat} ratio such as

$$E_{rat} = \left[\sum_i^{M_c} E_\perp \middle/ \sum_i^{M_c} E_\parallel \right]_{y_i \geq y_{c.m.}}, \quad (14)$$

where $E_\perp$ and $E_\parallel$ are the transverse and longitudinal kinetic energies in the center of mass, respectively. Large ratios are expected to correspond to highly central collisions, i.e., the so-called E_{rat}^5 cut defined as ≥ 0.75 at $150A$ MeV, which includes as many events as PM5 for a given set of collected events.

B. IMF distributions

The measured dM/dZ distributions, for Au+Au at $150A$ MeV, are shown in Fig. 1 for $(y \geq 0)_{c.m.}$ and several cuts on the PM. If the additional condition $(0 \leq y \leq 0.6y_P)_{c.m.}$ is imposed on the event rapidity, then one obtains the distributions shown in Fig. 2 in which the dM/dZ obtained with E_{rat}^5 but without the extra condition on y is also presented. The aim of these cuts is to restrict the analysis and entropy determination to a region of the phase space covering only particles which have been emitted from the most violent reactions. These particles are expected to have a high probability of being thermally and chemically equilibrated as stressed in earlier works [49,50]. The application of the $(0 \leq y \leq 0.6y_P)_{c.m.}$ cut allows the removal of the spectatorlike component, as can be readily seen in Fig. 3 of Ref. [11].
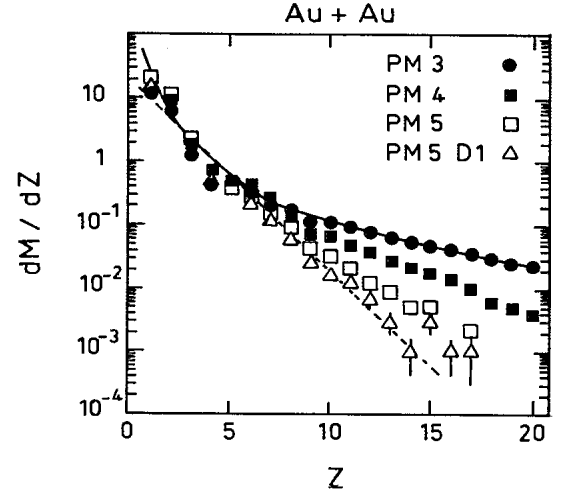

FIG. 1. dM/dZ multiplicity distributions of fragments, not corrected for efficiency effects (see text), measured in the Au+Au reaction at $150A$ MeV. The different distributions correspond to different criteria of centrality from semicentral (PM3,PM4) to very central PM5D1 (see Sec. IV A). The solid curve illustrates a power law $Z^{-\alpha}$ dependence, with $\alpha = 2.03$, and the dashed line represents an exponential falloff $e^{-\sigma Z}$, with $\sigma = 0.76$.

The error bars reported in Figs. 1 and 2 are of statistical origin. As a result of acceptance and low energy thresholds effects (which are Z dependent) characterizing the FOPI detector (see Sec. III), the yields should be actually raised by some amount. The lack of efficiency due to acceptance has been evaluated from filtered simula-
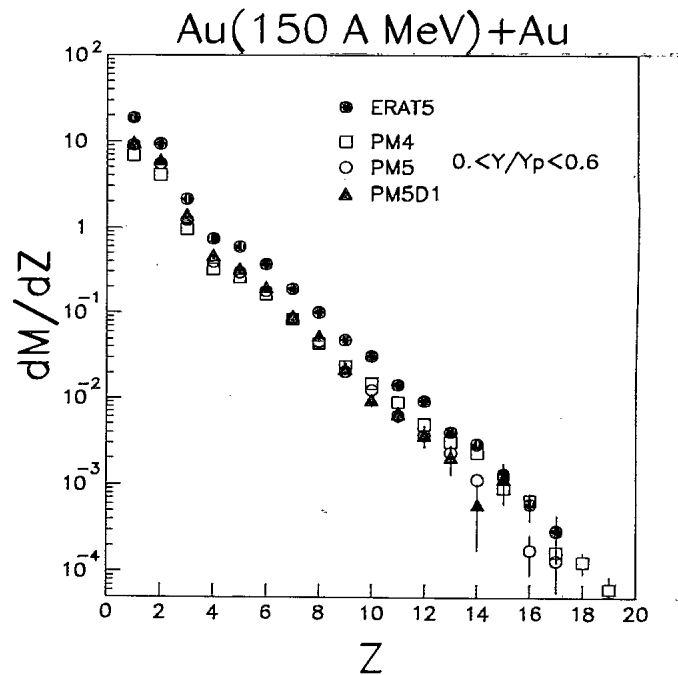

FIG. 2. Same as Fig. 1 with the $(0 \leq y \leq 0.6y_P)_{c.m.}$ extra condition on the rapidity y. This allows a more stringent selection of the nuclear system's participant zone. The distribution obtained with E_{rat}^5, another criterion of centrality with no condition on y (see text), is also shown.

tions with the quantum molecular dynamical model [9,51] to decrease from 20% to 5% over the $Z=1-4$ range; that due to energy thresholds is estimated to be less than 10% for $5 < Z < 10$. These corrections which if included would be practically invisible in Figs. 1 and 2 do not prevent us from making, from these figures, the following observations.

(1) The semicentral distributions (PM3,PM4) exhibit a two-slope trend due to the presence of heavy fragments related to remnants or to decay of the projectilelike part. The PM3 distribution may be fairly well reproduced with a power law dependence curve (solid curve in Fig. 1) of the $Z^{-\alpha}$ type with $\alpha=2.03$. In contrast, the more central distributions are characterized by a one-slope falloff of the $e^{-\sigma Z}$ type (dashed line) with $\sigma=0.76$. These two different behaviors illustrate the limitation inherent to inclusive measurements which average impact parameters and led earlier to the "extra-entropy puzzle" [19,35,37] and to the speculated liquid-vapor phase transition [22,52–54], which remains undiscovered so far.

(2) The extra condition on the rapidity, of course, reduces the multiplicities, but yields quite similar trends for PM5, PM5D1, and $E_{\rm rat}^5$ and brings PM4 quite close to the same tendency. This credits the effective ability of $E_{\rm rat}^5$ to select central reactions with a large fraction of participating nucleons.

(3) The absolute values of the multiplicity increase with centrality. This is easily understood since the size of the participant zone should grow as the impact parameter diminishes.

(4) The PM5D1 distribution extends up to $Z \sim 16$, the IMF ($Z > 2$) multiplicity is close to one-fifth of the total charged particle multiplicity, and moreover the charge carried by the IMF's nearly 30% of the total charge measured, thus stressing the importance of IMF's.

(5) The exponential falloff of the dM/dZ distribution agrees well with the trend predicted by statistical decay models such as the QSM [17].

(6) Since both the PM5D1 [with $(0 \leq y \leq 0.6 y_P)_{\rm c.m.}$] and the $E_{\rm rat}^5$ (without it) criteria exhibit comparable trends for the IMF distributions, both can be used to extract S/A. In the following analysis we have used the former criterion. *An identical analysis was performed with $E_{\rm rat}^5$; in that case the S/A values are found to be different by less than 5% than those presented here.*

V. DETERMINATION OF THE BARYONIC ENTROPY (S/A)

Before comparing the experimental multiplicities to those calculated with the QSM, the former have, first, to be extended to the whole space (4π) and to the full Au+Au system. Actually, the experimental multiplicities are for a participant zone which is reduced compared to the entire Au+Au system implied in the QSM calculations. An alternate method consisting of comparing directly the experimental dM/dZ to the filtered QSM calculations is not feasible here since the calculations are not performed in a Monte Carlo framework. This could be performed by using the computer code FREESCO [56]. However, comparisons of the predicted dM/dZ distribu-

tions with those presently measured for Au+Au show a somewhat unrealistic low yield for the higher Z's; hence, FREESCO has not been used in this analysis. The extrapolation to 4π was done by multiplying the experimental multiplicities by a factor $158/Z_{\rm tot}$ ($2Z_{\rm Au}=158$), where $Z_{\rm tot}$ is the total charge measured for the participant zone with the specific criterion of centrality used. Of course, by doing this one assumes that the $(N=236)/(Z=158)$ ratio, characterizing Au+Au, is preserved in the participant zone selected. The extrapolated multiplicities are reported in Fig. 3.

At this point it is important to notice that, due to pion emission [57], the N/Z ratio taken in the QSM calculations may be different from $(236/158)=1.49$. Solid information about the Au+Au system formed at the incident energies considered here is not available. The π^- yield per participant proton can be inferred from the compilation work of Stock [58]. It is less than 10^{-2} for bombarding energies lower than $400A$ MeV and of the order of 0.05 at $800A$ MeV, while the π^-/π^+ yield ratio is expected to vary like $(N/Z)^2$. This suggests that a de-
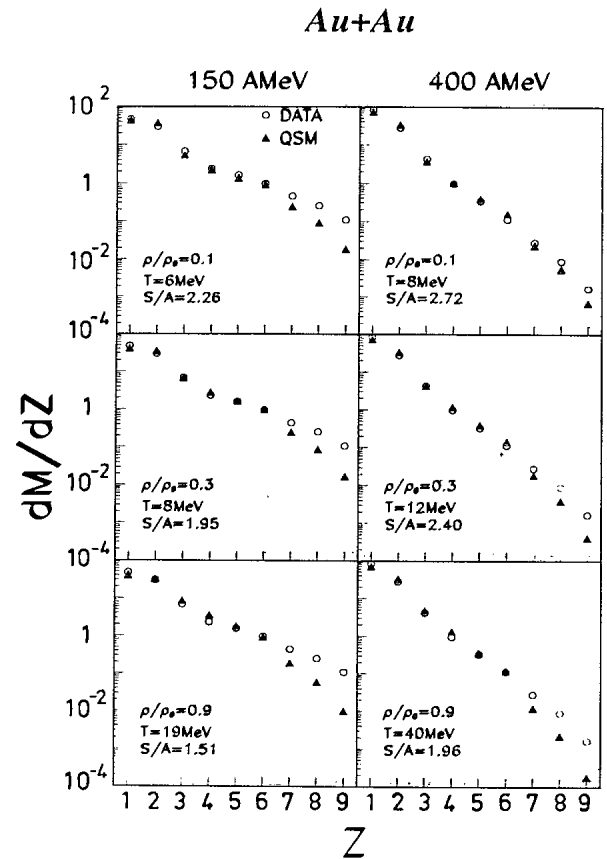
Au+Au

FIG. 3. Some examples of agreement found, for the Au+Au reaction at $150A$ and $400A$ MeV, between dM/dZ multiplicity distributions measured (open circles) and calculated (solid triangles) with the QSM. The experimental distributions have been "extrapolated" to the whole Au+Au system (see text). Calculations are shown for three different freeze-out densities $\rho/\rho_0=0.1$, 0.3, and 0.9, where ρ_0 is the saturation density. The corresponding temperature T and baryonic entropy S/A value predicted by the model for these cases are also indicated.

crease of about 5% of the N/Z ratio may be expected from pion emission. However, as a conservative attitude, we have run calculations in the case where ($N = 197$)/($Z = 197$) (to have the same nucleon multiplicities as for the actual Au+Au system); i.e., certainly the most extreme scenario one may think of. Differences of about 0.1 unit are observed between the S/A values calculated with $N/Z = 1.49$ and with $N/Z = 1$. As shown later on, these differences enter in the uncertainties characterizing the extracted baryonic entropy values and overall in those resulting from our missing knowledge about the freeze-out density. Nevertheless, these isotopic effects may not be negligible when considering specific particle ratios, as done in previous works [37,38].

The calculated dM/dZ distributions were obtained by varying T for a given ρ. Some examples of distributions at 150A and 400A MeV, corresponding to $\rho/\rho_0 = 0.1$, 0.3, and 0.9, which agree well, from visual comparison, with the experimental one are presented in Fig. 3. The agreement is generally quite satisfactory at least up to $Z \sim 7$ where the statistics have dropped by two orders of magnitude. Thus, from these comparisons, at each pro-

jectile energy and for each density, one can derive a temperature and an entropy per nucleon; both values are also given in Fig. 3. In order to judge of the accuracy of this visual comparison, we present in Fig. 4 examples of an experimental (circles) and two calculated (triangles) distributions corresponding both to $\rho/\rho_0 = 0.3$ but to two different temperatures ($T = 13$ and 16 MeV); the calculated S/A values are also reported in the figure. In the first case (upper frame), the agreement is good over the full distribution, while in the other case (lower), although a better agreement is achieved for $Z = 1$ and 2, a clear departure is observed for $Z > 2$. A difference of about 9% is found between the two S/A values. Furthermore, the comparison of the upper frame of Fig. 4 with the right-middle frame of Fig. 3, both illustrating a satisfactory agreement between measured and calculated distributions over the $1 \leq Z \leq 6$ range, yields a difference of $\approx 3\%$ for S/A. This suggests that, with such a method, the entropy can be determined with less than 5% uncertainties around $S/A \approx 2.5$. The comparisons presented in Figs. 3 and 4 are summarized in Fig. 5 where the extracted S/A values are displayed in the T-ρ/ρ_0 plane; some isentropic curves calculated with the QSM are also shown. At 150A MeV, for example, one sees that indeed S/A varies from a value slightly above 2 down to 1.5 as ρ/ρ_0 increases from 0.1 to 0.9. So far the freeze-out density is not known, but earlier works [25,39] suggest that ρ/ρ_0 could be around 0.3 and likely less than 0.5. We will keep this value of 0.3 throughout the article. How-
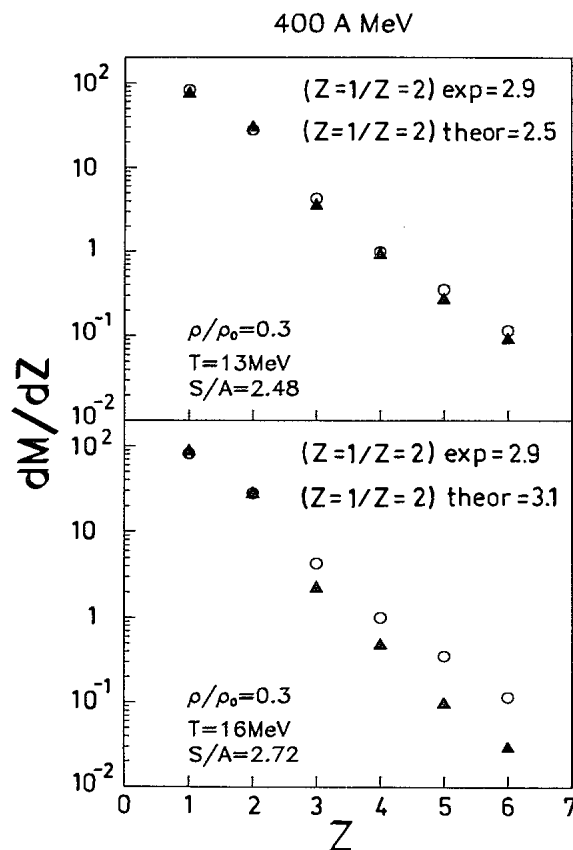

FIG. 4. Measured IMF multiplicity distributions "extrapolated" to the whole Au+Au system (open circles) and calculated with the QSM (solid triangles) for the Au(400A MeV)+Au reaction. In the calculations, the breakup density was taken as $\rho/\rho_0 = 0.3$ and two different temperatures $T = 13$ MeV (upper frame) and 16 MeV (lower) are considered; the corresponding S/A values are reported. The experimental $Z = 1-2$ yield ratio and those calculated with the QSM are also presented.
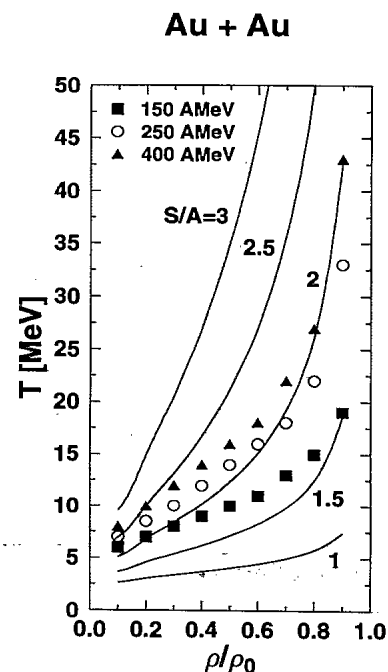

FIG. 5. Temperature versus freeze-out to saturation density ratio ρ/ρ_0 as determined from the comparison of the experimental dM/dZ distributions with those calculated with the QSM for the Au+Au reaction at the 150A, 250A, and 400A MeV. Some isentropic curves (constant S/A) calculated with the QSM, for $S/A = 1-3$ in steps of 0.5 unit, are also shown.

ever, it is worth noticing that, as shown in Fig. 5, S/A changes by not more than 0.2 when ρ/ρ_0 is varied below 0.5. Upper and lower values of the entropy obtained for $0.1 < \rho/\rho_0 < 0.9$ will also be presented at some points of the discussion to come.

In the following, instead of comparing systematically the calculated and measured dM/dZ distributions, we have made use of the various observables characterizing the distributions which are directly related to S/A in the framework of the QSM. We have used the multiplicity (M_{ap}) of all charged products $(Z \geq 1)$, the fragment $(Z \geq 3)$, multiplicity (M_f), the average charge of the fragments $(\langle Z_f \rangle)$, the slope parameter σ of the distributions, and some relative yield ratios of different species pertaining to the IMF distributions. The analyses have been performed at $150A$, $250A$, $400A$, $600A$, and $800A$ MeV incident energies. They include all fragments with $1 \leq Z \leq 15$ with the exception of the slope parameter determination method where only $1 \leq Z \leq 8$ were considered. Another method would consist of using the average mass of all products $(\langle A_{ap} \rangle)$. This is not feasible, in the present case, since only Z is measured. Yet the average charge of all products $(\langle Z_{ap} \rangle)$ might be utilized, but this latter would not yield an independent method since $\langle Z_{ap} \rangle$ is related to M_{ap} by the simple relation $\langle Z_{ap} \rangle = 158/M_{ap}$. Nevertheless, in order to examine the trend of M_{ap} as well as that of $\langle Z_{ap} \rangle$ as a function of S/A, we will present both in the following.

Let us remark that the consistency of the S/A values found with the different methods implies implicitly that the whole experimental dM/dZ distribution fully agrees with that calculated with the QSM. Furthermore, the comparison of the calculated with the measured observables yields S/A uncertainties less than those (estimated to be less than 5%) corresponding to the visual adjustment of the calculated to the measured Z distributions.

At this point it is important to make the following remark. Although it should be reiterated that the PM5D1 $+ (0 \leq y \leq 0.6y_P)_{c.m.}$ and E_{rat}^5 cuts are optimized ways to select particles participating in the most violent reactions, it is nevertheless very interesting to examine the evolution of the different observables listed above as a function of centrality. This is illustrated in Fig. 6 showing, as an example, the variation of four observables, measured at $400A$ MeV, as a function of the multiplicity bins. However, when the extra condition $(y \leq 0.6y_P)_{c.m.}$ is added, they exhibit only weak differences with no marked trend. This indicates that, irrespective of the centrality, if the true participant zone is correctly selected and not too small, the same entropy value should always be found.

Let us compare now the measured observables with those calculated with the QSM; this study is presented in Figs. 7, 8, and 10 and is summarized in Table I. The calculated total multiplicities of all charged products $(Z \geq 1)$ and that of fragments $(Z \geq 3)$ are shown as a function of S/A, for $\rho/\rho_0 = 0.3$, in Figs. 7(a) and 7(b), respectively. The former increases with S/A until it saturates at 158 $(Z_{Au} = 79)$; the second increases first to about 22 as the system breaks into a growing number of IMF's
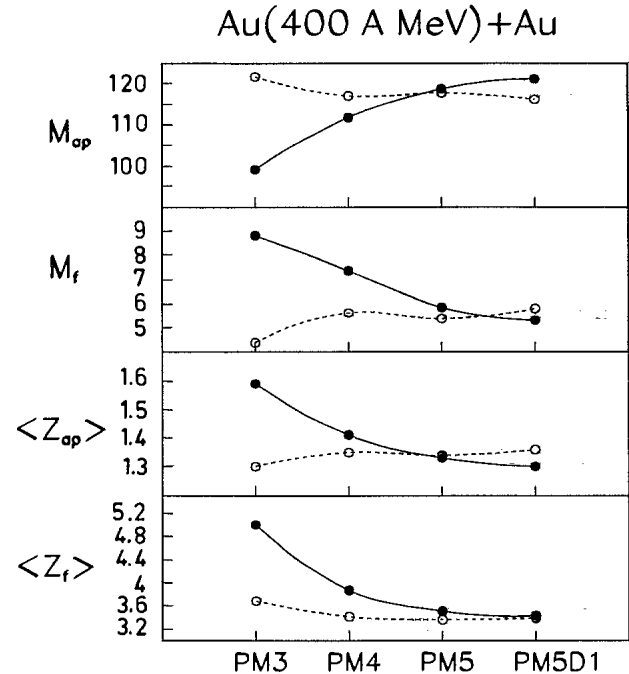

FIG. 6. "Extrapolated" multiplicity of all charged products (M_{ap}) and of $Z \geq 3$ fragments (M_f), average charge of all products $(\langle Z_{ap} \rangle)$ and average charge of fragments $(\langle Z_f \rangle)$ plotted as a function of the centrality in the Au($400A$ MeV)+Au reaction. The criterion of centrality (PM3-PM5D1) is explained in the text. The dots are for the selection condition based on the multiplicity bins alone. The open circles correspond to the case where the extra condition $(y \leq 0.6y_P)_{c.m.}$ on the rapidity is added. The solid and dashed curves are to guide the eye. As opposed to the dots which express a marked trend, the open circles reflect a fair constancy of all the observables.

which subsequently become lighter. Then, as S/A keeps rising, the number of $Z < 3$ clusters goes up accordingly; consequently, the $Z \geq 3$ fragment multiplicity starts to decrease. The experimental values (dots) are also shown in Fig. 7. At $150A$ MeV, for example, the multiplicities for $Z \geq 1$ and $Z \geq 3$ are found to be equal to 89.9 and 12.6, respectively; they yield S/A values of 1.98 and 1.94. Let us observe that the multiplicities vary rapidly with S/A; thus, they offer a sensitive determination of the baryonic entropy.

The calculated average charges of all emitted products $\langle Z_{ap} \rangle$ and that of fragments $\langle Z_f \rangle$ plotted against S/A are presented in Figs. 8(a) and 8(b). As readily expected, they diminish as S/A increases to saturate at 1 and 3, respectively. At $150A$ MeV, the experimental data allow the extraction of entropy values equal to 1.85 for IMF's (see Table I). In contrast to the method where M_{ap} and M_f are used, S/A varies here very rapidly with the average charges when these quantities get close to their minimum value. Thus, independent of the fact that M_{ap} and $\langle Z_{ap} \rangle$ do not provide alternate determinations of S/A, the observed trend shows that M_{ap} is more appropriate than $\langle Z_{ap} \rangle$ to determine the entropy in the domain where $S/A > 1.8$.

TABLE I. The baryonic entropy S/A determined, for the Au+Au reaction measured at the incident energies given in column 1, from the comparison of four different observables measured and calculated with the QSM for $\rho=0.3\rho_0$. The observables are the multiplicity M_{ap} of all charged products, the multiplicity M_f of the fragments $(Z \geq 3)$, the average charge $\langle Z_f \rangle$ of the fragments, and the slope coefficient σ of the dM/dZ multiplicity distribution fitted with $e^{-\sigma Z}$; they are reported in columns 2, 4, 6, and 8, respectively. The multiplicities M_{ap} and M_f are extended to the entire Au+Au system (see text). The S/A values extracted with the first three observables are typically affected by a $\pm 3\%$ error, while those from σ have a $\pm 7\%$ uncertainty attached. The $\langle S/A \rangle$ values have been obtained by averaging the S/A values reported in the previous columns. $\overline{S/A}$ represents the mean values obtained by averaging the S/A values determined, from the same four methods, for $\rho=0.1\rho_0$ and $\rho=0.9\rho_0$; $\overline{\Delta(S/A)}$ corresponds to the overall limits of $\overline{S/A}$ when ρ varies between $0.1\rho_0$ and $0.9\rho_0$.

E (MeV)	M_{ap}	S/A	M_f	S/A	$\langle Z_f \rangle$	S/A	σ	S/A	$\langle S/A \rangle$	$\overline{S/A} \pm \overline{\Delta(S/A)}$
150A	89.9	1.98	12.6	1.94	4.00	1.85	0.76	1.75	1.88	1.85±0.35
250A	106.5	2.30	8.33	2.25	3.55	2.20	1.16	2.15	2.22	2.21±0.34
400A	116.5	2.57	5.76	2.45	3.38	2.48	1.37	2.35	2.46	2.41±0.36
600A	124.4	2.78	4.2	2.57	3.32	2.65	1.58	2.55	2.63	2.60±0.36
800A	130.6	2.97	3.7	2.65	3.32	2.65	1.76	2.75	2.75	2.69±0.36

Next, it is also possible to determine the entropy from the slope parameter of the dM/dZ distributions assumed to be $e^{-\sigma Z}$. In the following, the slope parameters have been determined from a weighted least-squares fit to the data for $Z=1-8$. One example of a fit is given in Fig. 9 for 400A MeV; the slope parameter is found to be equal

to $\sigma=1.37$. These values (cf. Table I) are reported in Fig. 10 showing the dependence of S/A on the slope parameter of the distributions. As can be observed in this figure, for increasing S/A the slope parameter σ goes first through a kind of plateau before rising. This can be understood as follows: A low projectile energy creates low entropy; thus, the dM/dZ distributions contain a
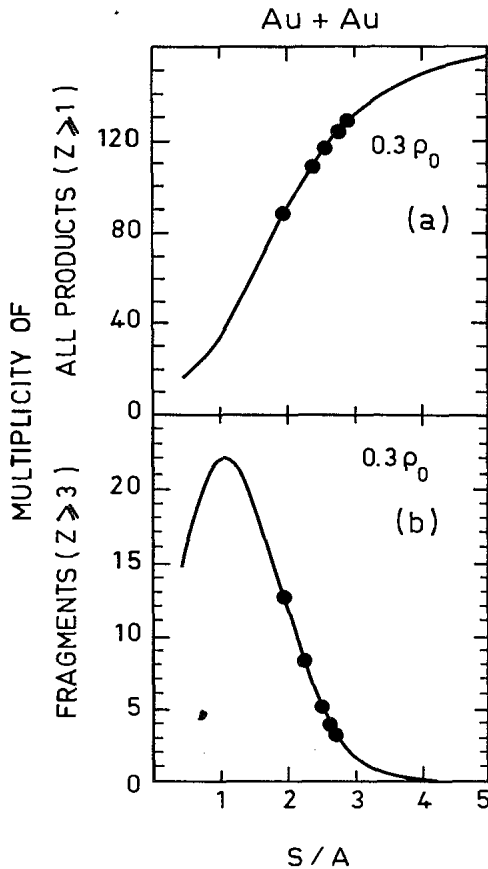

FIG. 7. Multiplicity (a) of all charged products $(Z \geq 1)$ and (b) of fragments $(Z \geq 3)$ emitted in the Au+Au reaction as a function of baryonic entropy S/A for $\rho/\rho_0=0.3$ calculated with the QSM. The experimental multiplicities "extrapolated" to the whole Au+Au system are reported by dots for the different incident energies.
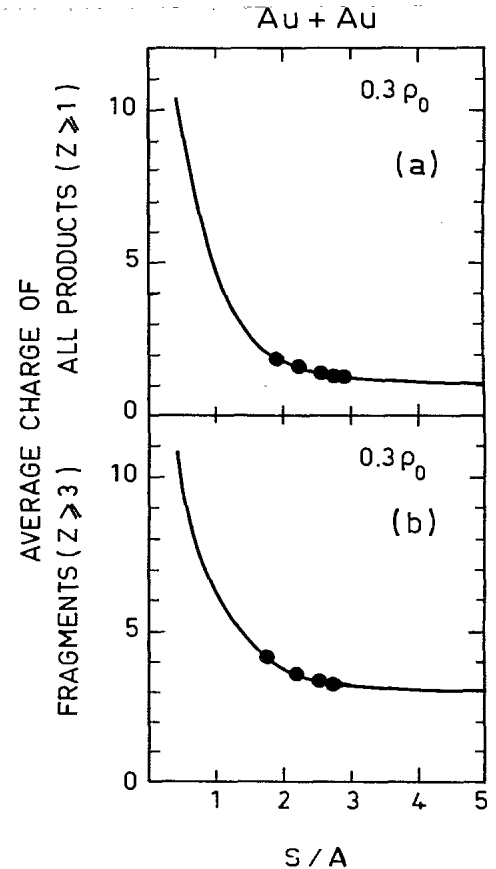

FIG. 8. Average charge (a) of all charged products $(Z \geq 1)$ and (b) of fragments $(Z \geq 3)$ emitted in the Au+Au reaction as a function of baryonic entropy S/A for $\rho/\rho_0=0.3$ calculated with the QSM. The average charge values extracted experimentally at the different incident energies are also reported (dots).
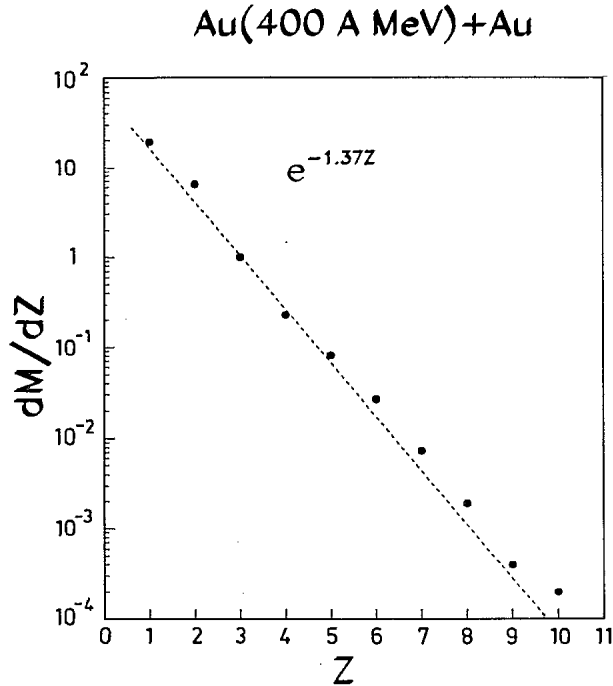
Au(400 A MeV)+Au

FIG. 9. dM/dZ multiplicity distribution measured (dots) for the Au+Au reaction at $400A$ MeV. The dotted line is a fit to the data assuming an exponential dependence $e^{-\sigma Z}$; σ is found to be equal to 1.37.

large variety of massive fragments and, hence, the fairly flat distribution for $Z=1-8$. As S/A rises, the distributions present an increasing light cluster component which produces a change of slope. From then on, as the average mass of the clusters diminishes and their multiplicity increases, the slope gets steeper. This method of entropy
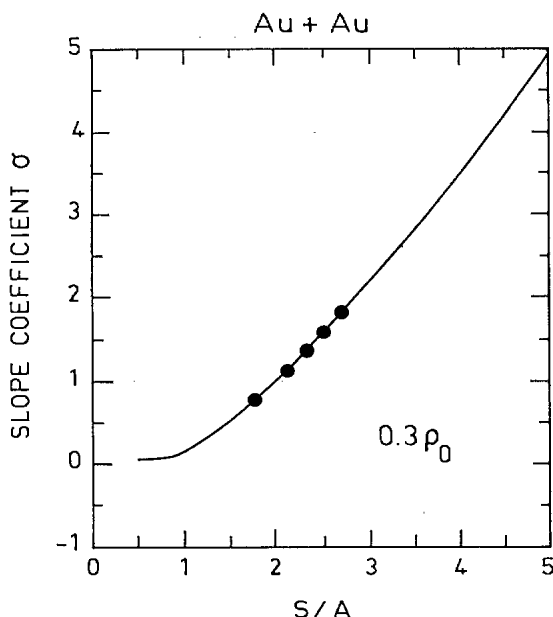
Au + Au

FIG. 10. Slope parameter σ of the dM/dZ multiplicity distributions calculated with the quantum statistical model as a function of baryonic entropy S/A for the Au+Au reaction assuming $\rho/\rho_0=0.3$. The experimental σ values obtained at different incident energies are also reported (dots).

extraction is, perhaps, a little more delicate to use than the previous methods, at least for lower energies, because the falloff is at variance with respect to a straight exponential dependence and also because the QSM departs from the experimental distribution for $Z \geq 7$ (see Fig. 3). The extracted entropies are found to be systematically slightly lower than those obtained from the previous methods.

Finally, S/A can also be extracted from the relative yields of different species. Such a method has been used in previous works [35,37-39] as a sensitive test of the QSM from the aspect of isospin and requires a mass determination for the light clusters and IMF's. In the present case, only a comparison of the calculated and measured $Z_i/(Z=1)$ and Z_i/Z_k ratios of a particular Z fragment to proton or of two particular species, respectively, can be made. We do not present here this analysis in detail. Nevertheless, one can easily infer from the concordance between measured and calculated dM/dZ distributions illustrated in Fig. 3 that quite a good agreement is obtained for all calculated and measured $Z \leq 6$ yields and hence for their ratio. Therefore the entropy values found in this way agree with those obtained with other methods.

Summing up, the S/A values obtained with the different observables, for $\rho/\rho_0=0.3$, are reported in Table I and appear to be quite consistent. For a given projectile energy, they depart from their average value $\langle S/A \rangle$ by about 0.15 at most. This remains true over the whole range of bombarding energy. The entropy values determined from M_{ap}, Z_{ap}, and Z_f are typically affected by a $\pm3\%$ uncertainty, while it is of $\pm7\%$ when using the slope coefficient σ. They result from statistical errors combined with systematic errors occurring over the treatment. The $\overline{S/A}$ values, given in column 11 of Table I, are obtained by averaging the $\langle S/A \rangle$ values corresponding to density $\rho/\rho_0=0.1$ and 0.9. They turn out to be very close to those extracted for $\rho/\rho_0=0.3$. The $\Delta(\overline{S/A})$ correspond to the overall limits of $\overline{S/A}$ for $\rho/\rho_0=0.1$ and 0.9. The S/A values show a fairly moderate increase over the $(150-800)A$ MeV energy range and tend to saturate around ~ 2.8. Such a trend is expected from dynamical calculations [17]; it was measured before, but the entropies extracted were found to be appreciably larger than in the present analysis. This point will be discussed in the next section.

VI. DISCUSSION

From the analysis presented before, one sees that on the whole $\langle S/A \rangle$ increases from 1.88 up to 2.75 (see Table I) over the $(150-800)A$ MeV energy domain. This excitation function is presented in Fig. 11 together with earlier Au+Au experimental results [38]; calculations corresponding to a thermal fireball source [55] and to hydrodynamics [59,60] are also displayed. The hatched zone delimits $\overline{S/A}+\Delta(\overline{S/A})$ values found experimentally by varying the freeze-out density from $\rho=0.1\rho_0$ up to $\rho=0.9\rho_0$. Within these limits, one sees that $\Delta(\overline{S/A})$ varies on the average by about ± 0.36.
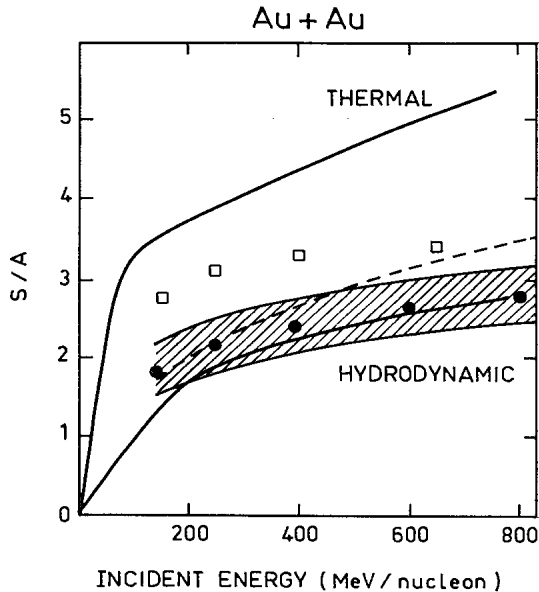
Au + Au

FIG. 11. Baryonic entropy S/A plotted as a function of incident energy. Earlier (open squares) and present (dots) experimental results for $\rho/\rho_0 = 0.3$ are reported. The hatched area illustrates the overall limits of the S/A values for a freeze-out density ρ varying between $0.1\rho_0$ and $0.9\rho_0$ (see Table I). The solid curve (labeled THERMAL) is for the fireball model [55]. Two hydrodynamic calculations are presented: One (solid curve) is deduced from a very hard equation of state [59]; the other (dashed curve) is from Ref. [60] and corresponds to a 3D fluid-dynamic calculation (see text).

Let us compare first the results with those previously obtained [38] at $150A$, $250A$, $400A$, and $650A$ MeV, a set of energies very similar to the present one. Both excitation functions exhibit the same tendency to rise, but the present values are systematically about 0.8 unit lower than those in Ref. [38]. The former S/A values were obtained from d, t, and ^{3,4}He to proton yield ratios for a finite reduced multiplicity N_p/N_p^{max}, where N_p is the number of protonlike part defined as in Eq. (3) but restricted to the participant and N_p^{max} is defined as in Ref. [45], i.e., the maximum protonlike multiplicity taken at the lower limit of the PM5 bin (see Sec. IV A). It is difficult to comment on the discrepancy between the two sets of entropy values because they were obtained from different methods. Here the approach closest to that used in Ref. [38] consists of measuring the $Z_i/(Z=1)$ ratios.

The S/A values found in the present work may be considered as quite reliable for the following reasons: (1) The participant zone is perhaps better selected with the PM5D1+$(0 \leq y \leq 0.6y_P)_{c.m.}$ criterion than with the $N_p/N_p^{max} = 1$ condition.

(2) The different observables used here lead to a very consistent set of S/A values which ascertains that the calculated dM/dZ distributions agree with the experimental ones over the whole range of Z.

(3) The fact that all Z species are taken into account is crucial and is illustrated in Fig. 4. In this figure, an example of a good agreement between experimental and

calculated $(Z=1)/(Z=2)$ yield ratios (lower frame) without ensuring that the complete calculated and measured dM/dZ distributions agree is shown. It yields a different S/A value than in the case (upper frame) where the agreement between measured and calculated Z_i/Z_k yield ratios is extended to all Z's.

(4) When the analysis is restricted to $Z < 3$, higher entropy values are generally found, without quite retrieving those obtained by Doss et al. [38]; such a fact was already observed in a previous work [61]. Let us also remark that varying the ρ/ρ_0 breakup density over the 0.1–0.9 range (hatched zone in Fig. 11) leaves the S/A values far below those found by Doss et al. At last, let us emphasize that points 2, 3, and 4 underline the relevance of IMF's in the entropy determination.

Doss et al. [38] have shown that S/A varies with N_p/N_p^{max}, i.e., the impact parameter, and decreases with rising centrality. They have also shown that, extrapolated to infinity, the entropy S^∞ would be substantially lower than those found for finite multiplicities and would thus be comparable with hydrodynamics calculations. In principle, the same problem exists here also. However, as opposed to the previous analysis, the S/A values found in the present work do not seem to depend much on the centrality of the collision, as illustrated in Fig. 6. This also qualifies somewhat the need of a large volume of nuclear matter in order to be entitled to derive an entropy, as well as the presumed volume dependence of the entropy. This finding implies that the entropy produced in the central reaction is determined by the incident energy only. Whether this holds true also in asymmetric systems remains to be investigated.

As mentioned in the Introduction, the isotopic distributions of light products [41] and those of neutrons [42] have been measured simultaneously with the IMF's in the present Au+Au experiment. They also allow S/A determination and will certainly bring further interesting information.

It is important to remark that the present entropy values staying below 3 at all energies correspond to Au+Au systems expanding along isentropes traversing, at low densities, the region of mechanical instability (spinodal, droplet) of a nuclear medium or the region where liquid and vapor phases may coexist [19].

Let us now turn to the comparison with model predictions shown in Fig. 11. As pointed out before, the fireball model [55], which assumes that all the initial center-of-mass energy is converted into thermal energy, fails totally to reproduce the data and demonstrates the importance of compression in relativistic heavy-ion reactions; i.e., the internal energy is shared into thermal and compression in approximately equal proportions as suggested by dynamical models [17,20] and preliminary results [62].

Good agreement is obtained with hydrodynamic predictions [59,60]. The solid curve, already shown by Doss et al., [38] corresponds to a very hard equation of state ($K = 550$ MeV). A three-dimensional (3D) fluid-dynamic calculation [60] (dashed curve) is also shown. In fact, it appears that S/A depends less strongly on the stiffness of the equation of state than on the shear viscosity (η). Some predictions of the baryonic entropy from viscous
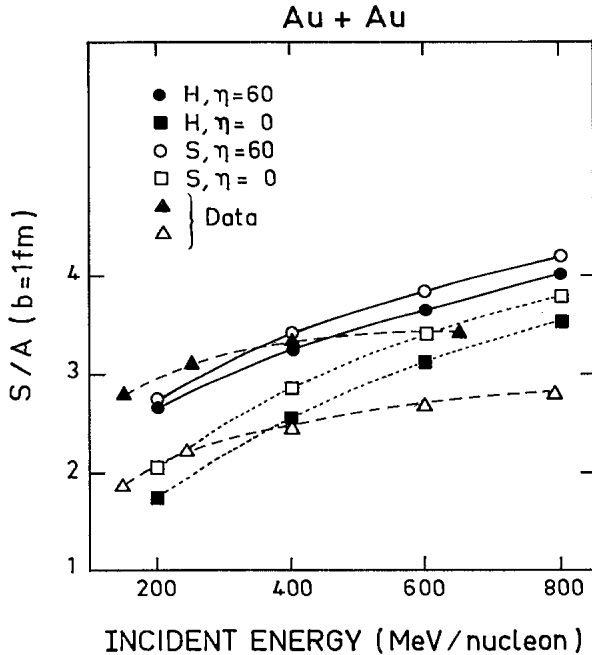
FIG. 12. Baryonic entropy S/A for central collisions ($b=1$ fm) obtained for hard ($H,K=400$ MeV) and soft ($S,K=160$ MeV) equations of state with viscous hydrodynamic calculations [60]. Two values of the shear viscosity coefficient $\eta=0$ and 60 MeV/fm$^2 c$ are considered for each stiffness of the equation of state. Experimental data from earlier [38] (solid triangles) and present (open triangles) works are reported. The curves are to guide the eye.

hydrodynamics calculation [60] are presented in Fig. 12 for Au+Au ($b=1$ fm). Curves for hard ($H,K=400$ MeV) and soft ($S,K=160$ MeV) equations of state with shear viscosity ($\eta=60$ MeV/fm$^2 c$) and without ($\eta=0$) are shown; the H and $\eta=0$ curve corresponds to the dashed one in Fig. 11. Their comparison with the data suggests a rather weak shear viscosity which has to be compared to $\eta \lesssim 30$ MeV/fm$^2 c$ as yielded by microscopic calculations for infinite matter [63,64]. On the other hand, the results of Doss et al. [38] would indicate a larger shear viscosity close to 60 MeV/fm$^2 c$. Bulk viscosity, assumed to be weak [60] at these incident energies, has not been considered here. Figure 12 seems also to indicate that an equation of state with a viscosity depending on the initial energy put into the system should perhaps be suitable. Let us remark that a variation of ρ within the $0.1\rho_0$ and $0.9\rho_0$ limits (hatched area in Fig. 11) does not change the overall conclusion neither about the trend of S/A as a function of incident energy nor about its deficit with respect to earlier measurements nor about the good agreement with hydrodynamics.

Having determined the baryonic entropy for a particular density $\rho/\rho_0=0.3$, it is tempting to extract a tempera-

ture value. Returning to Figs. 3 and 5, one sees that, according to the QSM, such a density corresponds to temperatures varying between 8 and 12 MeV over the range spanning $150A$ and $400A$ MeV. These temperatures are low compared to general expectations based on hydrodynamics [17,65] since these calculations show that $E^{\text{therm}} \sim \frac{1}{2}E_{\text{c.m.}}$; hence, T should be appreciably larger. Rather low temperatures were also measured in an earlier work [39] of a similar nature. Figures 3 and 5 show that T depends strongly on ρ; this suggests that only direct and independent measurements of either T or ρ will allow a reliable determination of these observables. Some attempts are now in progress [62,66,67].

VII. SUMMARY

In this article we have presented some results obtained for the Au+Au reaction, performed at $150A$, $250A$, $400A$, $600A$, and $800A$ MeV projectile energies, with the FOPI detector at GSI. By relying upon the assumption that hot and compressed systems formed in relativistic heavy-ion reactions expand almost isentropically after the entropy has been produced almost entirely at the early stage of the compression phase, we have extracted baryonic entropy values for the Au+Au system. This was done by measuring various observables characterizing the dM/dZ multiplicity distributions of emitted fragments from the participant zone of the colliding system and by comparing them with those predicted by the quantum statistical model [17,20]. This model has established the relevance of the intermediate mass fragments for a correct determination of the entropy and offers alternate methods for extracting it. In the present work, all the emitted products from $Z=1$ up to ~ 15 have been taken into account for the first time for determining the entropy. The different methods that have been used yield very consistent S/A values whose average varies, assuming a freeze-out density $\rho=0.3\rho_0$, from ~ 1.9 up to ~ 2.8 between $150A$ and $800A$ MeV. Extending ρ/ρ_0 to the overall limits 0.1–0.9 yields average $\overline{S/A}$ values very close to those found for $\rho/\rho_0=0.3$ with $\Delta(S/A) \sim \pm 0.36$. The entropies extracted here are somewhat lower than those obtained in earlier studies where the IMF's were not actually taken into account. The present values are in satisfactory agreement with hydrodynamic expectations and suggest a weak shear viscosity of nuclear matter. Only a direct determination of the temperature or of the freeze-out density will yield, via S/A measurements, a reliable determination of these observables; such attempts are in progress.

[1] For a review, see *The Nuclear Equation of State,* Vol. 216 of *NATO Advanced Study Institute, Series B: Physics,* edited by W. Greiner and H. Stöcker (Plenum, New York, 1989).

[2] H. Stöcker and W. Greiner, Phys. Rep. **137**, 277 (1986).

[3] W. Scheid, H. Müller, and W. Greiner, Phys. Rev. Lett. **32**, 741 (1974).

[4] R. B. Clare and D. Strottman, Phys. Rep. **141**, 177 (1986).

[5] G. F. Bertsch, H. Kruse, and S. Das Gupta, Phys. Rev. C **29**, 675 (1985).

[6] H. Kruse, B. V. Jacak, J. J. Molitoris, G. D. Westfall, and H. Stöcker, Phys. Rev. C **31**, 1770 (1985).

[7] G. F. Brugio, P. Chomaz, and J. Randrup, Phys. Rev. Lett. **69**, 885 (1992).

[8] C. Grégoire, B. Remaud, F. Sébille, L. Vinet, and Y. Raffray, Nucl. Phys. **A465**, 317 (1987).

[9] J. Aichelin and H. Stöcker, Phys. Rev. Lett. B **176**, 14 (1986).

[10] P. J. Siemens and J. I. Kapusta, Phys. Rev. Lett. **43**, 1486 (1979).

[11] J. P. Alard and the FOPI Collaboration, Phys. Rev. Lett. **69**, 889 (1992).

[12] N. Herrmann for the FOPI Collaboration, Nucl. Phys. **A553**, 739c (1993).

[13] P. J. Siemens and J. O. Rasmussen, Phys. Rev. Lett. **42**, 880 (1979).

[14] M. I. Sobel, P. J. Siemens, J. P. Bondorf, and H. A. Bethe, Nucl. Phys. **A251**, 502 (1975).

[15] G. Bertsch, Nucl. Phys. **A400**, 221c (1983).

[16] K. K. Gudima, V. D. Toneev, G. Röpke, and H. Schulz, Phys. Rev. C **32**, 1605 (1985).

[17] D. Hahn and H. Stöcker, Nucl. Phys. **A476**, 718 (1988).

[18] G. Bertsch and J. Cugnon, Phys. Rev. C **24**, 2514 (1981).

[19] H. Stöcker, G. Buchwald, G. Graebner, P. Subramanian, J. A. Maruhn, W. Greiner, B. V. Jacak, and G. D. Westfall, Nucl. Phys. **A400**, 63c (1983).

[20] D. Hahn and H. Stöcker, Phys. Rev. C **37**, 1048 (1988).

[21] L. P. Csernai, J. I. Kapusta, G. Fai, D. Hahn, J. Randrup, and H. Stöcker, Phys. Rev. C **35**, 1297 (1987).

[22] L. P. Csernai and J. Kapusta, Phys. Rep. **131**, 223 (1986), and references therein.

[23] J. Randrup and S. E. Koonin, Nucl. Phys. **A356**, 223 (1981); see also Nucl. Phys. **A474**, 173 (1987).

[24] G. Fai and J. Randrup, Nucl. Phys. **A381**, 557 (1982); see also Nucl. Phys. **A404**, 551 (1983).

[25] J. P. Bondorf, R. Donangelo, I. N. Mishustin, C. J. Pethick, H. Schulz, and K. Sneppen, Nucl. Phys. **A443**, 321 (1985); see also Nucl. Phys. **A444**, 460 (1985).

[26] D. H. E. Gross, Zhang Xiao-ze, and Xu Shu-yan, Phys. Rev. Lett. **56**, 1544 (1986); see also Phys. Lett. **161B**, 47 (1985); Rep. Prog. Phys. **53**, 605 (1990).

[27] D. H. E. Gross, in Proceedings of the XXXI International Winter Meeting on Nuclear Physics, Bormio, Italy, 1993, edited by I. Tori, Ricerca Scientifica ed Educazione Permanente, Supplemento No. 96 (1993), p. 80.

[28] A. S. Botvina, A. S. Iljinov, I. N. Mishustin, J. P. Bondorf, R. Donangelo, and K. Sneppen, Nucl. Phys. **A475**, 663 (1987); see also Nucl. Phys. **A507**, 649 (1990).

[29] M. Blann, T. T. Komoto, and I. Tserruya, Phys. Rev. C **40**, 2498 (1984).

[30] M. Blann, M. G. Mustafa, G. Peilert, H. Stöcker, and W. Greiner, Phys. Rev. C **44**, 431 (1991); see also Phys. Rev. Lett. **54**, 2215 (1985); Phys. Rev. C **32**, 1231 (1985).

[31] W. A. Friedman and W. G. Lynch, Phys. Rev. C **28**, 16 (1983).

[32] C. Barbagallo, J. Richert, and P. Wagner, Z. Phys. A **324**, 97 (1986).

[33] S. Nagamiya, M. C. Lemaire, E. Möller, S. Schnetzer, G. Shapiro, H. Steiner, and I. Tanihata, Phys. Rev. C **24**, 971 (1981).

[34] B. V. Jacak, G. D. Westfall, C. K. Gelbke, L. H. Harwood, W. G. Lynch, D. K. Scott, H. Stöcker, M. B. Tsang, and T. J. M. Symons, Phys. Rev. Lett. **51**, 1846 (1983).

[35] H. H. Gutbrod, H. Löhner, A. M. Poskanzer, T. Renner, H. Riedesel, H. G. Ritter, A. Warwick, F. Weik, and H. Wieman, Phys. Lett. **127B**, 317 (1983).

[36] B. V. Jacak, H. Stöcker, and G. D. Westfall, Phys. Rev. C **29**, 1744 (1984).

[37] K. G. R. Doss, H. A. Gustafsson, H. H. Gutbrod, B. Kolb, H. Löhner, B. Ludewigt, A. M. Poskanzer, T. Renner, H. Riedesel, H. G. Ritter, A. Warwick, and H. Wieman, Phys. Rev. C **32**, 116 (1985).

[38] K. G. R. Doss, H. A. Gustafsson, H. H. Gutbrod, D. Hahn, K. H. Kampert, B. Kolb, H. Löhner, A. M. Poskanzer, H. G. Ritter, H. R. Schmidt, and H. Stöcker, Phys. Rev. C **37**, 163 (1988).

[39] R. Wada, K. D. Hildenbrand, U. Lynen, W. F. J. Müller, H. J. Rabe, H. Sann, H. Stelzer, W. Trautmann, R. Trockel, N. Brummund, R. Glasow, K. H. Kampert, R. Santo, E. Eckert, J. Pochodzalla, I. Bock, and D. Pelte, Phys. Rev. Lett. **58**, 1829 (1987).

[40] J. P. Coffin for the FOPI Collaboration at GSI, Int. J. Mod. Phys. E: Reports on Nucl. Phys., Vol. 1 No. 4, 739 (1992).

[41] G. Poggi, M. Bini, A. Olmi, P. Maurenzig, G. Pasquali, and N. Taccetti, in Proceedings of the 7th Adriatic International Conference on Nuclear Physics, Islands of Brioni, Croatia, 1991, edited by R. Caplar and W. Greiner (World Scientific, Singapore, in press), p. 293.

[42] The LAND Collaboration (private communication).

[43] F. Ajzenberg-Selove, Nucl. Phys. **A360**, 1 (1981); **A375**, 1 (1982); **A392**, 1 (1983); **A415**, 1 (1984); **A433**, 1 (1985).

[44] A. Gobbi and the FOPI Collaboration at GSI, Nucl. Instrum. Methods **A324**, 156 (1993).

[45] K. G. R. Doss, H. A. Gustafsson, H. H. Gutbrod, K. H. Kampert, B. Kolb, H. Löhner, B. Ludewigt, A. M. Poskanzer, H. G. Ritter, H. R. Schmidt, and H. Wieman, Phys. Rev. Lett. **57**, 302 (1986).

[46] P. Beckmann, H. A. Gustafsson, H. H. Gutbrod, K. H. Kampert, B. Kolb, H. Loehner, A. M. Poskanzer, H. G. Ritter, H. R. Schmidt, and T. Siemiarczuk, Mod. Phys. Lett. A **2**, 163 (1987).

[47] R. Bock, G. Claesson, K. G. R. Doss, R. L. Ferguson, I. Gavron, H. A. Gustafsson, H. H. Gutbrod, J. W. Harris, B. V. Jacak, K. H. Kampert, B. Kolb, P. Kristiansson, F. Lefebvres, A. M. Poskanzer, H. G. Ritter, H. R. Schmidt, T. Siemiarczuk, L. Teitelbaum, M. Tincknell, S. Weiss, H. Wieman, and J. Wilhelmy, Mod. Phys. Lett. A **2**, 721 (1987).

[48] W. Reisdorf for the FOPI Collaboration, in Proceedings of the XX International Workshop on Gross Properties of Nuclei and Nuclear Excitation, Hirschegg, Austria, 1992, edited by H. Feldmeier (GSI and Institut für Kernphysik, Technische Hochschule, Darmstadt, 1992), p. 38.

[49] G. Peilert, H. Stöcker, W. Greiner, A. Rosenhauer, A. Bohnet, and J. Aichelin, Phys. Rev. C **39**, 1402 (1989).

[50] H. Stöcker and J. Konopka (private communication).

[51] J. Aichelin, Phys. Rep. **202**, 233 (1991).

[52] R. W. Minich, S. Agarwal, A. Bujak, J. Chuang, J. E. Finn, L. J. Gutay, A. S. Hirsch, N. T. Porile, R. P. Scharenberg, B. C. Stringfellow, and F. Turkot, Phys. Lett. **118B**, 458 (1982).

[53] A. D. Panagiotou, M. W. Curtin, H. Toki, D. K. Scott, and P. J. Siemens, Phys. Rev. Lett. **52**, 496 (1984).

[54] A. S. Hirsch, A. Bujak, J. E. Finn, L. J. Gutay, R. W. Minich, N. T. Porile, R. P. Scharenberg, B. C. Stringfellow, and F. Turkot, Phys. Rev. C **29**, 508 (1984).

[55] J. Gosset, H. H. Gutbrod, W. G. Meyer, A. M. Poskanzer, A. Sandoval, R. Stock, and G. D. Westfall, Phys. Rev. C **16**, 629 (1977); see also Phys. Rev. Lett. **37**, 1202 (1976).

[56] G. Fai and J. Randrup, Comput. Phys. Commun. **42**, 385 (1986).

[57] J. I. Kapusta, Phys. Rev. C **16**, 1493 (1977).

[58] R. Stock, Phys. Rep. **135**, 259 (1986).

[59] H. Stöcker, M. Gyulassy, and J. Boguta, Phys. Lett. **103B**, 269 (1981).

[60] W. Schmidt, U. Katscher, B. Waldhauser, J. A. Maruhn, H. Stöcker, and W. Greiner, Phys. Rev. C **47**, 2782 (1993).

[61] L. P. Csernai, G. Fai, and G. D. Westfall, Phys. Rev. C **38**, 2681 (1988).

[62] S. C. Jeong and the FOPI Collaboration and J. Randrup Phys. Rev. Lett. (submitted).

[63] P. Danielewicz, Phys. Lett. **146B**, 168 (1984).

[64] B. Schürmann, Mod. Phys. Lett. A **3**, 1137 (1988).

[65] D. Hahn and H. Stöcker, Nucl. Phys. **A452**, 723 (1986).

[66] C. Kuhn and the FOPI Collaboration and J. Konopka, in Proceedings of the XXXI International Winter Meeting on Nuclear Physics, Bormio, Italy, 1993, edited by I. Iori, Ricerca Scientifica ed Educazione Permanente, Supplemento No. 96 (1993), p. 53.

[67] T. Wienold, Ph.D. thesis, Universität Heidelberg (1993).